CORA Cork Open Research Archive
Cartlann Taighde Oscailte Chorcaí

Title	ReS2/Si 2D/3D vertical heterojunction as a self-powered photodiode
Authors	Intonti, Kimberly;Pelella, Aniello;Neill, Hazel;Patil, Vilas;Hurley, Paul K.;Ansari, Lida;Gity, Farzan;Di Bartolomeo, Antonio
Publication date	2024-10-24
Original Citation	Intonti, K., Pelella, A., Neill, H., Patil, V., Hurley, P. K., Ansari, L., Gity, F. and Di Bartolomeo, A. (2024) 'ReS2/Si 2D/3D vertical heterojunction as a self-powered photodiode', Applied Physics Letters, 125(17), 173505. https://doi.org/10.1063/5.0231243
Type of publication	Article (peer-reviewed)
Link to publisher's version	https://doi.org/10.1063/5.0231243
Rights	© 2024, the Authors. Published under an exclusive license by AIP Publishing. This article may be downloaded for personal use only. Any other use requires prior permission of the authors and AIP Publishing. This article appeared as: Intonti, K., Pelella, A., Neill, H., Patil, V., Hurley, P. K., Ansari, L., Gity, F. and Di Bartolomeo, A. (2024) 'ReS2/Si 2D/3D vertical heterojunction as a self-powered photodiode', Applied Physics Letters, 125(17), 173505, and may be found at:https://doi.org/10.1063/5.0231243
Download date	2024-11-10 02:08:56
Item downloaded from	https://hdl.handle.net/10468/16604

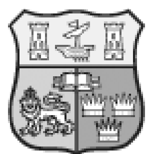

UCC
University College Cork, Ireland
Coláiste na hOllscoile Corcaigh

AIP Publishing
Applied Physics Letters
ACCEPTED MANUSCRIPT
This is the author's peer reviewed, accepted manuscript. However, the online version of record will be different from this version once it has been copyedited and typeset.
PLEASE CITE THIS ARTICLE AS DOI: 10.1063/5.0231243

ReS_2/Si 2D/3D Vertical Heterojunction as a Self-Powered Photodiode

Kimberly Intonti[1,2*], Aniello Pelella[3], Hazel Neill[4], Vilas Patil[4], Paul K. Hurley[4,5], Lida Ansari[4], Farzan Gity[4*], and Antonio Di Bartolomeo[1,2]

[1]*Department of Physics "E. R. Caianiello", University of Salerno, via Giovanni Paolo II, Fisciano, Salerno, 84084, Italy*

[2]*CNR-SPIN Salerno, via Giovanni Paolo II, Fisciano, 84084, Italy*

[3]*Department of Physics, University of Roma "Tor Vergata", Via Della Ricerca Scientifica, 1 - 00133, Rome, Italy*

[4]*Tyndall National Institute, University College Cork, Lee Maltings, Dyke Parade, Cork, T12 R5CP, Ireland*

[5]*School of Chemistry, University College Cork, Cork, Ireland*

Corresponding authors' e-mail: kintonti@unisa.it ; farzan.gity@tyndall.ie

ABSTRACT

2D/3D van der Waals heterostructures provide an excellent platform for high-performance optoelectronic systems by combining the intrinsic properties of 2D and 3D materials. In this study, we fabricate and study a type II ReS_2/Si van der Waals 2D/3D vertical heterojunction with multi-mode photodetection. In the dark, the heterojunction exhibits diode-like behaviour with a low reverse current and a high rectification ratio of ~10^3. Under illumination, the device shows a linear response to the light intensity. The ReS_2/Si photodetector exhibits stable and repeatable switching behaviour and can be operated in self-powered mode with a responsivity of about 0.10 mA/W at 10 mW incident power and a time response of 300 μs. Based on first-principles calculations, we propose a model to elucidate the photoconduction mechanisms occurring in the ReS_2/Si heterostructure.

AIP Publishing Applied Physics Letters ACCEPTED MANUSCRIPT
This is the author's peer reviewed, accepted manuscript. However, the online version of record will be different from this version once it has been copyedited and typeset.
PLEASE CITE THIS ARTICLE AS DOI: 10.1063/5.0231243

In the last decades, novel semiconductor nanostructures have been investigated for high-performance photodetectors[1–4]. Among them, bidimensional (2D) transition metal dichalcogenides (TMDs) have attracted much interest because of their large specific surface area, thickness-dependent bandgap, and strong light-matter interaction, which enables the realization of photoconductors and phototransistors with high photoresponsivity[5–10]. However, due to limited mobility, the speed of TMD-based devices is usually limited by the long transit time of photogenerated carriers, the existence of intrinsic defects[11,12] and the persistent photoconductivity[13].

Vertical heterojunction photodiodes provide an alternative to improve the device response speed because the photogenerated carriers can be easily separated and transported by the strong built-in electric field at the junction interface[14–16]. Several combinations of 2D TMDs with other 2D materials have been proposed[17,18] because their lack of dangling bonds and ability to interact through van der Waals (vdW) forces enable the creation of heterostructures (Hs) without lattice distortion[19,20]. For instance, 2D-2D vdW Hs such as MoS_2/WS_2[21] and MoS_2/BP[22,23] have demonstrated great photodetection performances. However, the fabrication techniques of 2D-2D heterojunctions, which are usually prepared by stacking CVD or exfoliated flakes, do not make them suitable for large-scale manufacturing. Furthermore, precise control over the doping type, carrier concentration, and stoichiometry of 2D materials is challenging, which in turn limits the device polarity[24]. Finally, the insufficient light absorption resulting from the ultrathin thickness of 2D materials usually leads to a limited external quantum efficiency[24].

The 2D/3D van der Waals heterostructures combine the advantages of both 2D layered materials and traditional 3D bulk materials offering a platform to design new multifunctional photodetectors[25–27]. Traditional 3D semiconductors have experienced long-term development, and their growth and device fabrication techniques are mature. However, although high-quality multilayer heterogeneous structures can be produced using conventional epitaxial techniques, it is challenging for epitaxy material with different lattice structures to grow together. Lattice mismatches lead to various defects that can increase the generation and recombination rates, even when a buffer layer is employed. Consequently, large dark currents, high noise, and low response speed are obtained[28].

2D/3D mixed-dimensional photodetectors have become a new research hotspot since they can provide a high-quality vdW Hs, ultrabroad detecting band, and strong light-absorption capacity[1,27,28].

AIP Publishing Applied Physics Letters ACCEPTED MANUSCRIPT
This is the author's peer reviewed, accepted manuscript. However, the online version of record will be different from this version once it has been copyedited and typeset.
PLEASE CITE THIS ARTICLE AS DOI: 10.1063/5.0231243

For instance, Zhang et al. achieved wide-spectrum detection from 200 nm to 1550 nm by realizing a high-quality vdW Hs made of WSe_2 grown in situ on n-Si[29]. An outstanding responsivity up to 117 A/W was achieved in MoS_2/Si photodetectors[30], and response times of the order of microseconds were measured for $MoSe_2$/Si heterostructures[31]. Besides, other TMDs such as $MoTe_2$ and WS_2, combined with Si exhibited huge potential as high-performance photodetectors[32–34].

As an interesting TMD semiconductor, rhenium disulfide (ReS_2) mainly differs from other TMDs as it maintains a direct bandgap, which goes from 1.35 eV as a bulk to 1.5 eV as a monolayer, irrespective of the number of layers, as well as an almost invariant band structure[35]. Because of its weak interlayer coupling, it shows in bulk form the electrical and vibrational properties of decoupled monolayers. These features make ReS_2 an attractive option for photodetection for both direct bandgap-enhanced photogeneration and the potential to use thicker flakes for higher light absorption[36,37].

Herein, we investigate a 2D/3D ReS_2-Si heterojunction as a self-driven photodetector.

The large area 2D ReS_2 flakes were mechanically exfoliated and subsequently transferred onto a low-doped n-type Si substrate. The elemental composition of the exfoliated flakes was analysed through Energy-dispersive X-Ray Spectroscopy (EDX). The spectrum of the large area flake used for the fabrication of the device is reported in Figure 1a. The concentrations of Re and S confirm a stoichiometric ratio of about 1:2, indicating that the quality of the original crystal was preserved during the exfoliation. The Atomic Force Microscopy (AFM) profile, reported in Figure 1b, reveals a 219 nm thick flake. The large thickness helps against the low light absorption issue of vertical 2D material-based devices[38]. Indeed, light absorption might be less than 10% if the thickness is below 100 nm[28]. The optical image in Figure 1c shows that the metal contact is completely contained within the flake area. The area of the circular metal pad is around 2100 μm^2, while the triangular-shaped flake has an area around 7800 μm^2. Figure 1d depicts a not-to-scale schematic representation of the device together with the measurement set-up.

The current transport through the heterostructure was investigated through I-V measurements, firstly performed in the dark and at room temperature. Figure 1e reports the typical I-V curve (blue line) of the Ni/ReS_2/Si structure measured in the dark, compared to the same characteristic (red line) of a reference Ni/Si Schottky diode. Compared to the Ni/Si diode, the Ni/ReS_2/Si structure exhibits a rectifying behaviour with a lower current at negative biases and a higher on-off current ratio. The reverse current, indeed, is about 4.1 nA and it is almost constant for negative biases. The rectification

Applied Physics Letters ACCEPTED MANUSCRIPT
This is the author's peer reviewed, accepted manuscript. However, the online version of record will be different from this version once it has been copyedited and typeset.
PLEASE CITE THIS ARTICLE AS DOI: 10.1063/5.0231243
AIP Publishing

ratio is about $7x10^2$ at ±1 V, which is higher than the one reported for other 2D/3D heterojunctions[34,39]. The small turn-on voltage of 0.16 V is extracted from the I-V curve in Figure 1e on a linear scale. Nearly ohmic contact of Ni to ReS_2 was previously confirmed (see supplementary material Sec 1), indicating that the ReS_2/Si junction is primarily responsible for the diode-like characteristic. Figure 1f shows the I-V curves of the ReS_2/Si structure at temperatures T in the 293-393 K range. The I-V curves become more symmetric with increased temperature, causing a reduction in the rectification ratio. The increase of the current with temperature both at positive and negative biases suggests that a temperature-activated electronic transport above an energy barrier occurs, such as a thermionic emission or thermionic field emission[40,41]. ReS_2 is a natural n-type semiconductor[35]. Therefore, the n-ReS_2/n-Si junction is a heterostructure where carrier transport is dominated by majority carriers, i.e. electrons. Thus, assuming a homogeneous barrier in the temperature range under investigation[42], the thermionic emission current equation can be applied[26,43] as described in supplementary material Sec 2, and an effective energy barrier around Φ_B = 0.32 eV can be extracted [41,44,45].

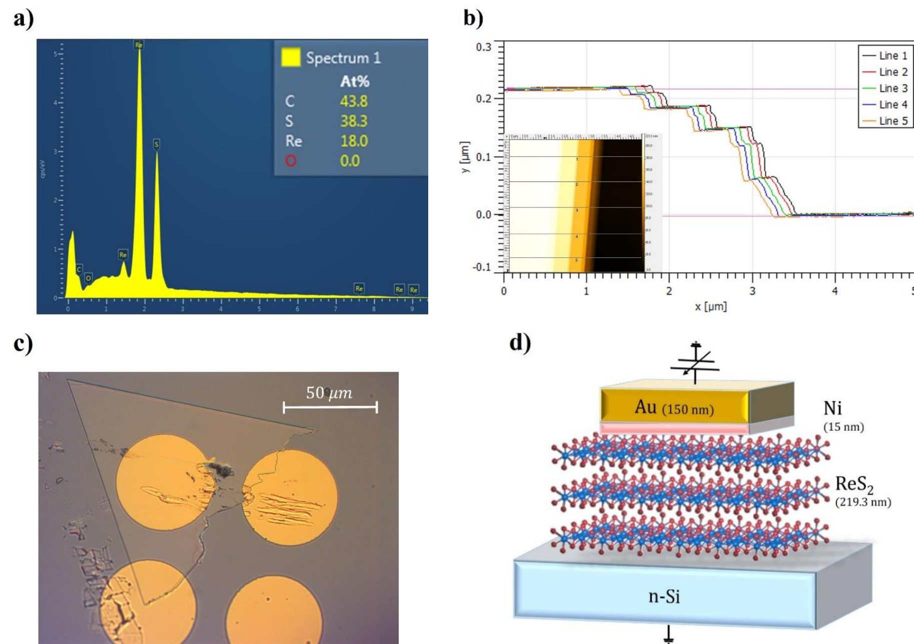

Applied Physics Letters ACCEPTED MANUSCRIPT
This is the author's peer reviewed, accepted manuscript. However, the online version of record will be different from this version once it has been copyedited and typeset.
PLEASE CITE THIS ARTICLE AS DOI: 10.1063/5.0231243
AIP Publishing

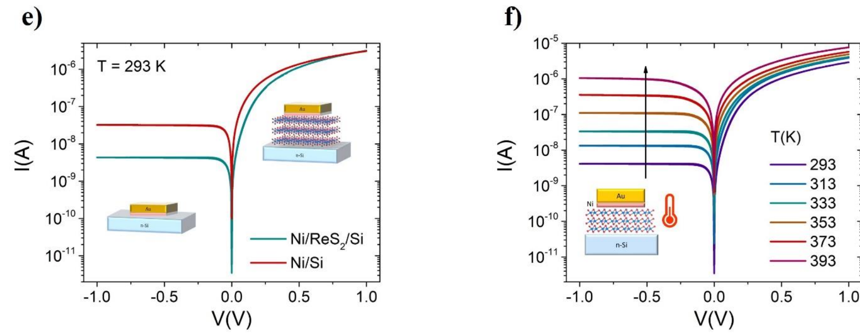

Figure 1. a) A representative EDX spectrum of the ReS_2 flake. b) AFM profile across the edge of the flake. The inset shows the AFM image. c) Optical image of the device under test. d) Schematic 3D structure of the device, with the measurement set up. e) Comparison between the I-V curves of the Ni/ReS_2/Si structure and the Ni/Si Schottky diode, in the dark and at room temperature. f) I-V curves of the Ni/ReS_2/Si device measured at different temperatures, from 293 to 393 K.

Supplementary material Sec 3 reveals that, under a white supercontinuum laser with a maximum nominal absolute power of 110 mW, the embedded ReS_2 layer in the Ni/ReS_2/Si heterostructure enables a photocurrent, defined as

$$I_{ph} = I_{light} - I_{dark},$$

which is almost one order of magnitude greater than the one measured for the Ni/Si junction, at negative biases. In the following, the photoresponse features are provided as a function of the incident power P_{inc} that considers both the size of the light spot A_{spot} and the effective exposed area of the flake A_{flake}, rather than the absolute power P. It is calculated as:

$$P_{inc} = \frac{P}{A_{spot}} A_{flake}.$$

Since the metal electrode on top of the ReS_2 flake (see Figure 1c) is not transparent and reflects most of the light, the effective light-sensitive area A_{flake} is assumed to be the flake area exceeding the metal contact, which is completely exposed to the light from the optical fiber.

Figure 2a depicts the I-V curves of the ReS_2/Si device measured at different P_{inc} = 0.10 to 10.2 mW. Although the current increases under both positive and negative bias conditions, the latter results in much higher photo-to-dark current ratios I_{ph}/I_{dark} with a maximum of around 10^2, indicating better charge separation[46].

AIP Publishing Applied Physics Letters ACCEPTED MANUSCRIPT
This is the author's peer reviewed, accepted manuscript. However, the online version of record will be different from this version once it has been copyedited and typeset.
PLEASE CITE THIS ARTICLE AS DOI: 10.1063/5.0231243

Most photodetector applications need the extraction of the detected light intensity from the photocurrent across a broad range of light intensities; therefore, having a linear dependence of the photocurrent on the laser intensity is highly desirable. The linear dynamic range (LDR) identifies the light intensity range where the photodetectors show a constant responsivity. It is expressed as:

$$\mathrm{LDR} = 20 \log \frac{\mathrm{P_{sat}}}{\mathrm{P_{low}}}$$

Where P_{sat} and P_{low} represent the maximal and minimum light intensities, respectively, at which the photocurrent start deviating from linearity[47].

As highlighted by Figure 2b and 2c, I_{ph} follows a linear trend ($I_{ph} \sim P^{\alpha}$, with $\alpha \simeq 1$) across the whole light intensity range here investigated, both at positive and negative biases; a wider range has to be considered to have a clear deviation from a linear trend. Therefore, considering the strongest and the weakest incident powers as P_{sat} and P_{low}, the LDR value is roughly 40.

Many literature works report α values lower than 1 for 2D TMD/3D devices, indicating that the photogeneration/recombination processes are mediated by traps/defects [33,48]. The obtained $\alpha \simeq 1$ points out the good quality of the material in the present study.

The linear I_{ph}-P_{inc} relationship results in a nearly constant photoresponsivity of about (0.15 ± 0.01) mA/W and (0.028 ± 0.003) mA/W at V= 0.5 and -0.5 V respectively, as shown in Figure 2b and 2c. It was calculated as follows

$$\mathrm{R} = \mathrm{I_{ph}}/\mathrm{P_{inc}}.$$

Responsivity maps as a function of the external bias and power intensity are reported in supplementary material Sec 4.

Figure 2d shows the current of the ReS_2/Si heterostructure in response to sequences of light pulses, each obtained by turning on and off the laser with a period of one second and repeated at different powers. When the device is illuminated, the current increases, and it returns to its dark value when illumination is turned off, exhibiting a steep rise and decay. Moreover, the heterojunction shows a stable, rapid photoresponse and reversible photoswitching over multiple cycles, and the photocurrent is easily modulated by changing the incident power. A similar pulse sequence but at V = -0.5 V is reported in supplementary material Sec 5.

Applied Physics Letters ACCEPTED MANUSCRIPT
This is the author's peer reviewed, accepted manuscript. However, the online version of record will be different from this version once it has been copyedited and typeset.
PLEASE CITE THIS ARTICLE AS DOI: 10.1063/5.0231243
AIP Publishing

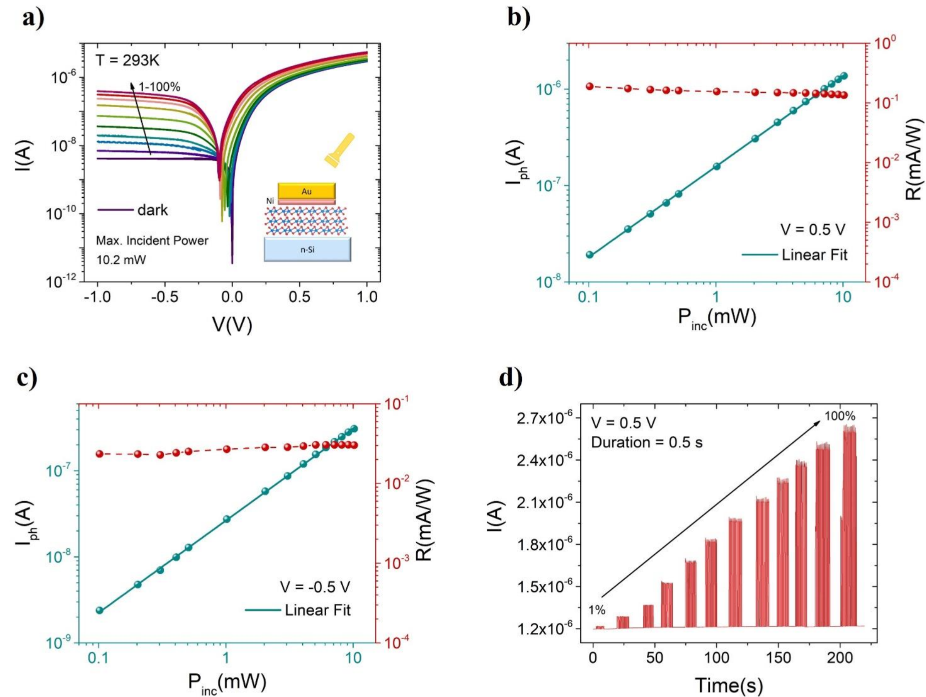

Figure 2. Photoresponse of the ReS_2/Si device: a) I-V curves on semi-log scale measured under illumination by a supercontinuum white laser at increasing incident optical power, compared with the I-V measured in the dark. b,c) Log-log plot of the photocurrent, and the correspondent responsivity, as a function of the incident optical power at b) positive and c) negative bias. d) Switching response of the device with 1s-period, under increasing optical incident power.

From Figure 2a, it is also evident that the device can be operated in self-powered mode. Self-driven devices are indispensable for optoelectronics; thanks to their high photoresponse, 2D materials based self-driven photodetectors have recently gathered significant attention[49,50].

To deeply investigate this operating condition, the device response to laser pulses of different intensities was recorded at zero external bias voltage, and zero external current, as shown in Figure 3a. The short-circuit current I_{sc} increases with the laser intensity by following a linear trend as a function of the incident power, with an LDR about 40, as shown in Figure 3b. This result suggests an effective photo-charge separation and possibly a band offset modification in the heterojunction

AIP Publishing Applied Physics Letters ACCEPTED MANUSCRIPT
This is the author's peer reviewed, accepted manuscript. However, the online version of record will be different from this version once it has been copyedited and typeset.
PLEASE CITE THIS ARTICLE AS DOI: 10.1063/5.0231243

because of light absorption. At the maximum incident power of 10.2 mW, I_{sc} reaches the high value of 0.1 µA.

The open circuit voltage V_{oc} increases with the increasing incident power as well, achieving the absolute value $|V_{oc}| = 0.1$ V under the maximum incident power. The I_{ph}/I_{dark} ratio, being the dark current about 1 pA, reaches a value of $5x10^4$ as reported in Figure 3c, indicating a high self-driven capability of the photodetector, comparable to other homopolar 2D/3D heterostructures like n-MoS_2/n-GaAs[51], n-$MoTe_2$/n-Si[32]. Tuning the device structure and investigating a wider range of light intensities might be necessary to achieve detectivity and responsivity competitive with those reported in other works[33,52]. Indeed, the effective responsivity ranges from 0.04 to 0.10 mA/W, while the effective detectivity D* in the visible light range, calculated as

$$D^* = \frac{R\sqrt{A}}{\sqrt{2qI_d}}$$

reaches $1x10^8$ Jones.

A fast-photoswitching response (see supplementary material Sec 6 for more details) is confirmed in Figure 3d by the rise and decay times of 300 and 500 µs, respectively.

AIP Publishing Applied Physics Letters ACCEPTED MANUSCRIPT
This is the author's peer reviewed, accepted manuscript. However, the online version of record will be different from this version once it has been copyedited and typeset.
PLEASE CITE THIS ARTICLE AS DOI: 10.1063/5.0231243

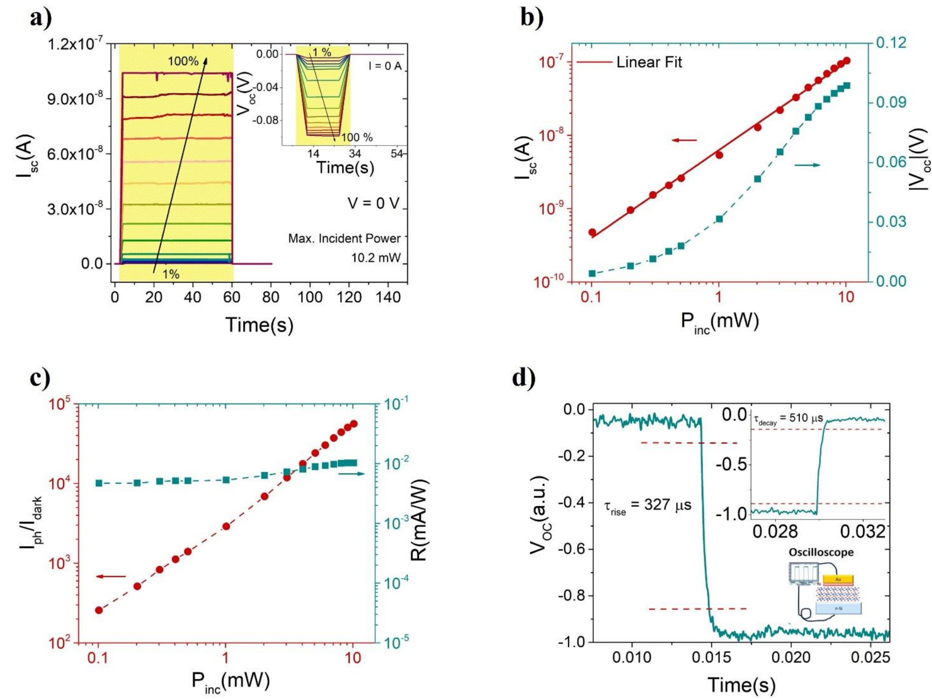

Figure 3. Photovoltaic behaviour of the ReS_2/Si device: a) Short circuit current I_{sc} and open circuit voltage V_{oc} (inset) under laser pulses of increasing incident power. b) I_{sc} and V_{oc} as a function of the incident optical power. Symbols are the data, the dashed line is an eye guide, while the solid line represents the linear fit of I_{sc}. c) Photocurrent over dark current ratio I_{ph}/I_{dark} (on the left) and responsivity R (on the right) vs. incident optical power P_{inc}. d) Rise and decay times extracted from the device's response to a light pulse.

To provide insight into the carrier transport mechanism through the Ni/ReS_2/Si heterostructure, we performed density functional theory (DFT) and nonequilibrium Green's function (NEGF) calculations as implemented in QuantumATK[53] (see supplementary material Sec 7). The planar-averaged charge density difference (CDD), atomic structure and energy-resolved local DoS (LDoS) across the ReS_2/Si and Ni/Si junctions are plotted in Figure 4 and in supplementary material Sec 8, respectively. LDoS is obtained with both sides of the junction held at equilibrium, and the Fermi level is shown by the dashed yellow line. As shown by the orange dashed lines in the LDoS profile at the ReS_2/Si interface, the Si conduction and valence bands bend 650 meV upwards near the junction. In the ReS_2 side of the junction, a rather small downward band bending of ~ 110 meV is observed in the ReS_2 side of

AIP Publishing Applied Physics Letters ACCEPTED MANUSCRIPT
This is the author's peer reviewed, accepted manuscript. However, the online version of record will be different from this version once it has been copyedited and typeset.
PLEASE CITE THIS ARTICLE AS DOI: 10.1063/5.0231243

the junction. The resulting band offset at the conduction band at the ReS_2/Si interface is ~ 0.72 eV, while the conduction band offset at the Ni/Si interface is ~ 0.3 eV. The ideal interface under consideration, excluding certain smoothing effects that result in the effective barrier established through experimentation, can explain discrepancies with experimental results. In the fabricated device, there is a strong probability that some atoms of the Si surface are not passivated, leading to the presence of dangling bonds. These dangling bonds are anticipated to strongly impact the ReS_2/Si band offset, especially since both the Si and the ReS_2 are n-type. Further, the calculated band offset from LDoS is under equilibrium, while it is expected that the application of an external electric field reduces the band offset [54].

The CDD is obtained as the difference between the total valence charge density and a superposition of neutral atom valence charge density at each atomic site. To estimate the dipole at the junctions, the macroscopic planar-average of the CDD has been extracted as shown in Figure 4, where the same distance at either side of each sampling grid point is considered in the macroscopic averaging scheme. + and – indicate the direction of the electron transfer at the interfaces; i.e., from Si to ReS_2 at the ReS_2/Si and from Ni to Si at the Ni/Si junctions. As expected, a larger value of charge transfer has been obtained for the Ni/Si junction compared to the ReS_2/Si structure.

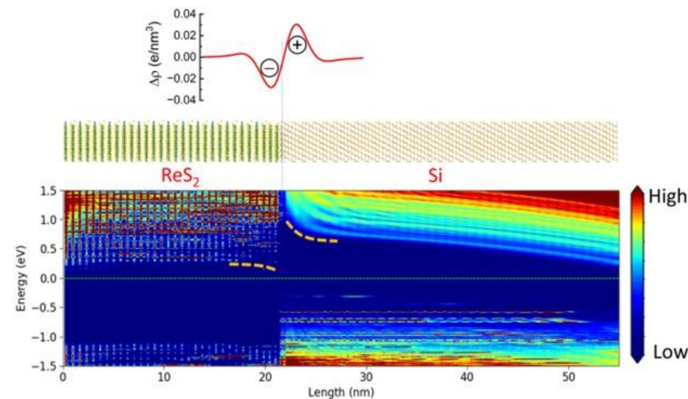

Figure 4. Planar-averaged CDD, atomic structure and energy-resolved LDoS of (top) ReS_2/Si.

DFT calculations and experimental results were used to elucidate the operating mechanism of the junction, represented in the band diagrams in Figure 5.

Figure 5a shows that ReS_2 and Si form a type II N-n heterojunction at equilibrium: in accordance with DFT simulation (see Figure 4), a depletion region occurs in the Si-side and an accumulation region is

AIP Publishing Applied Physics Letters ACCEPTED MANUSCRIPT
This is the author's peer reviewed, accepted manuscript. However, the online version of record will be different from this version once it has been copyedited and typeset.
PLEASE CITE THIS ARTICLE AS DOI: 10.1063/5.0231243

formed in the ReS_2 part. As mentioned before, the transport mechanism of the heterojunction is dominated by electrons, differently from what occurs in a p-n junction where minority carriers play an important role.

When a negative bias is applied to the Ni contact, the electron transport is limited by the energy barrier at the ReS_2/Si interface. Under illumination, photogenerated electrons move from ReS_2 to Si, while holes are transferred to the ReS_2 part and collected by the top electrode, contributing to the negative photocurrent, as shown in Figure 5b.

If the junction is positively biased, electrons experience a low barrier at the Si side and flow from the Si substrate towards ReS_2, as plotted in Figure 5c. Under illumination, the current increases moderately because electron-hole pairs which effectively contribute to the photocurrent are mostly generated in the depletion layer, reduced by the applied bias.

When no bias is applied, the measurements under illumination indicate the presence of a positive current in short-circuit condition and a negative voltage in open-circuit condition. This behaviour could be due to photogenerated electrons in the depletion region of Si that, being more energetic, move towards ReS_2, despite the built-in electric field, as represented in Figure 5d. Electrons at the ReS_2 side experience, instead, the ReS_2/Si barrier.

A reduction of band-bending at zero external bias at the Si interface under illumination could also account for this effect [55–57]. A positive photovoltage caused by holes produced by light adsorption in the depletion region and accumulated at the interface could provide a forward biasing of the heterojunction, giving a positive I_{sc}.

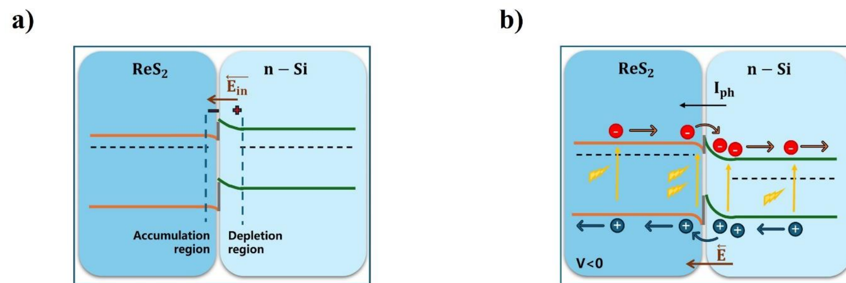

Applied Physics Letters ACCEPTED MANUSCRIPT

This is the author's peer reviewed, accepted manuscript. However, the online version of record will be different from this version once it has been copyedited and typeset.

PLEASE CITE THIS ARTICLE AS DOI: 10.1063/5.0231243

AIP Publishing

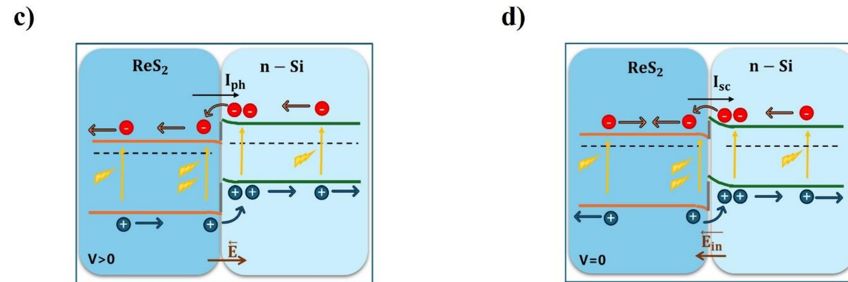

Figure 5. Band diagrams representing the dominant current mechanisms: a) in an equilibrium condition, in the dark; b) under negative external bias on the top contact, c) under positive external bias on the top contacts, d) under zero external bias. b), c) and d) represent the situation under illumination.

In conclusion, we reported the electrical characterization in the dark and under a laser source of a type II ReS_2/Si heterojunction. In the dark, the ReS_2/Si device exhibits a low reverse current of $4.1\text{x}10^{-9}$ A and a high rectification ratio of ~10^3, indicating a high-quality heterostructure. The photocurrent follows a linear trend with the power intensity and reaches high values in the order of the µA. The device can operate in self-powered mode with an I_{ph}/I_{dark} ratio of about 10^4 under external zero-bias voltage. A rise time of 300 µs and fall time of 500 µs have been extracted from its transient behaviour. Through DFT calculations, a detailed energy band model is proposed. The studied device is promising for high-throughput networks, fast optical switching, and optical communication.

SUPPLEMENTARY MATERIAL

See the Supplementary material file for details about the Ni/Si and the Ni/ReS_2 barrier, the device's photoresponse, the material's photovoltaic properties, the DFT calculations and the experimental details.

ACKNOWLEDGEMENT

V.P., P.K.H., L.A. and F.G. acknowledge the financial support from Science Foundation Ireland AMBER Research Centre (SFI-12/RC/2278_P2). H.N. acknowledges funding through Irish Research Council (IRC) EPSPG/2023/1772 project. This work was partially supported by the European Union’s Horizon 2020 project

ACCEPTED MANUSCRIPT
Applied Physics Letters
AIP Publishing
This is the author's peer reviewed, accepted manuscript. However, the online version of record will be different from this version once it has been copyedited and typeset.
PLEASE CITE THIS ARTICLE AS DOI: 10.1063/5.0231243

ASCENT+ (grant agreement no 871130). The SFI/HEA Irish Centre for High-End Computing (ICHEC) is acknowledged for the provision of computational facilities and support.

AUTHOR DECLARATIONS

Conflict of Interest

The authors have no conflicts to disclose

DATA AVAILABILITY

The data that support the findings of this study are available from the corresponding author upon reasonable request.

REFERENCES

(1) Li, H.; Yang, Z. Recent Progress in Mid-Infrared Photodetection Devices Using 2D/nD (N=0, 1, 2, 3) Heterostructures. *Materials & Design* **2023**, *225*, 111446. https://doi.org/10.1016/j.matdes.2022.111446.

(2) Zheng, Y.; Cao, B.; Tang, X.; Wu, Q.; Wang, W.; Li, G. Vertical 1D/2D Heterojunction Architectures for Self-Powered Photodetection Application: GaN Nanorods Grown on Transition Metal Dichalcogenides. *ACS Nano* **2022**, *16* (2), 2798–2810. https://doi.org/10.1021/acsnano.1c09791.

(3) Anter, A.; Orhan, E.; Ulusoy, M.; Polat, B.; Yıldız, M.; Kumar, A.; Di Bartolomeo, A.; Faella, E.; Passacantando, M.; Bi, J. Lanthanum(III)Hydroxide Nanoparticles and Polyethyleneimine-Functionalized Graphene Quantum Dot Nanocomposites in Photosensitive Silicon Heterojunctions. *ACS Appl Mater Interfaces* **2024**, *16* (17), 22421–22432. https://doi.org/10.1021/acsami.4c02102.

(4) Wang, P.; Liu, S.; Luo, W.; Fang, H.; Gong, F.; Guo, N.; Chen, Z.-G.; Zou, J.; Huang, Y.; Zhou, X.; Wang, J.; Chen, X.; Lu, W.; Xiu, F.; Hu, W. Arrayed Van Der Waals Broadband Detectors for Dual-Band Detection. *Advanced Materials* **2017**, *29* (16), 1604439. https://doi.org/10.1002/adma.201604439.

(5) Grillo, A.; Faella, E.; Pelella, A.; Giubileo, F.; Ansari, L.; Gity, F.; Hurley, P. K.; McEvoy, N.; Di Bartolomeo, A. Coexistence of Negative and Positive Photoconductivity in Few-Layer $PtSe_2$ Field-Effect Transistors. *Adv. Funct. Mater.* **2021**, *31* (43), 2105722. https://doi.org/10.1002/adfm.202105722.

(6) Ahmed, A.; Zahir Iqbal, M.; Dahshan, A.; Aftab, S.; Hegazy, H. H.; Yousef, E. S. Recent Advances in 2D Transition Metal Dichalcogenide-Based Photodetectors: A Review. *Nanoscale* **2024**, *16* (5), 2097–2120. https://doi.org/10.1039/D3NR04994A.

(7) Intonti, K.; Faella, E.; Viscardi, L.; Kumar, A.; Durante, O.; Giubileo, F.; Passacantando, M.; Lam, H. T.; Anastasiou, K.; Craciun, M. F.; Russo, S.; Di Bartolomeo, A. Hysteresis and Photoconductivity of Few-Layer ReSe2 Field Effect Transistors Enhanced by Air Pressure. *Advanced Electronic Materials n/a* (n/a), 2300066. https://doi.org/10.1002/aelm.202300066.

(8) Li, X.; Aftab, S.; Hussain, S.; Kabir, F.; Al-Sehemi, A. G.; Aslam, M.; Kim, J. H.; Goud, B. S. Progress in Photodetector Devices Utilizing Transition Metal Dichalcogenides. *J. Mater. Chem. C* **2024**, *12* (4), 1211–1232. https://doi.org/10.1039/D3TC04253G.

(9) Pelella, A.; Intonti, K.; Durante, O.; Kumar, A.; Viscardi, L.; De Stefano, S.; Romano, P.; Giubileo, F.; Neill, H.; Patil, V.; Ansari, L.; Roycroft, B.; Hurley, P. K.; Gity, F.; Di Bartolomeo, A. Multilayer WS2 for Low-Power Visible and near-Infrared Phototransistors. *Discover Nano* **2024**, *19* (1), 57. https://doi.org/10.1186/s11671-024-04000-0.

AIP Publishing Applied Physics Letters ACCEPTED MANUSCRIPT
This is the author's peer reviewed, accepted manuscript. However, the online version of record will be different from this version once it has been copyedited and typeset.
PLEASE CITE THIS ARTICLE AS DOI: 10.1063/5.0231243

(10) Malik, M.; Iqbal, M. A.; Choi, J. R.; Pham, P. V. 2D Materials for Efficient Photodetection: Overview, Mechanisms, Performance and UV-IR Range Applications. *Frontiers in Chemistry* **2022**, *10*.

(11) Intonti, K.; Coleman, E.; Blake, A.; Lyons, C.; Hydes, A.; Di Bartolomeo, A.; Gity, F.; Hurley, P. K. Role of Interface and Bulk Traps on the Capacitance–Voltage Characteristics of WS2/Al2O3/Si Capacitors. *Solid-State Electronics* **2023**, *207*, 108697. https://doi.org/10.1016/j.sse.2023.108697.

(12) Vancsó, P.; Magda, G. Z.; Pető, J.; Noh, J.-Y.; Kim, Y.-S.; Hwang, C.; Biró, L. P.; Tapasztó, L. The Intrinsic Defect Structure of Exfoliated MoS2 Single Layers Revealed by Scanning Tunneling Microscopy. *Sci Rep* **2016**, *6* (1), 29726. https://doi.org/10.1038/srep29726.

(13) Di Bartolomeo, A.; Genovese, L.; Foller, T.; Giubileo, F.; Luongo, G.; Croin, L.; Liang, S.-J.; Ang, L. K.; Schleberger, M. Electrical Transport and Persistent Photoconductivity in Monolayer MoS_2 Phototransistors. *Nanotechnology* **2017**, *28* (21), 214002. https://doi.org/10.1088/1361-6528/aa6d98.

(14) Han, Y.; Jiao, S.; Jing, J.; Chen, L.; Shi, Z.; Rong, P.; Wang, D.; Gao, S.; He, W.; Wang, J. Vertical Heterojunction Photodetector with Self-Powered Broadband Response and High Performance. *Chemical Engineering Journal* **2023**, *477*, 147060. https://doi.org/10.1016/j.cej.2023.147060.

(15) Capista, D.; Lozzi, L.; Di Bartolomeo, A.; Giubileo, F.; Martucciello, N.; Passacantando, M. SWCNT-Si Photodetector with Voltage-Dependent Active Surface. *Nano Ex.* **2024**, *5* (1), 015004. https://doi.org/10.1088/2632-959X/ad12d9.

(16) Liu, C.; Guo, J.; Yu, L.; Li, J.; Zhang, M.; Li, H.; Shi, Y.; Dai, D. Silicon/2D-Material Photodetectors: From near-Infrared to Mid-Infrared. *Light Sci Appl* **2021**, *10* (1), 123. https://doi.org/10.1038/s41377-021-00551-4.

(17) Yao, J.; Yang, G. Van Der Waals Heterostructures Based on 2D Layered Materials: Fabrication, Characterization, and Application in Photodetection. *Journal of Applied Physics* **2022**, *131* (16), 161101. https://doi.org/10.1063/5.0087503.

(18) Zhong, J.; Wu, B.; Madoune, Y.; Wang, Y.; Liu, Z.; Liu, Y. PdSe2/MoSe2 Vertical Heterojunction for Self-Powered Photodetector with High Performance. *Nano Res.* **2022**, *15* (3), 2489–2496. https://doi.org/10.1007/s12274-021-3745-9.

(19) Huang, M.; Li, S.; Zhang, Z.; Xiong, X.; Li, X.; Wu, Y. Multifunctional High-Performance van Der Waals Heterostructures. *Nature Nanotech* **2017**, *12* (12), 1148–1154. https://doi.org/10.1038/nnano.2017.208.

(20) Khan, S.; Khan, A.; Azadmanjiri, J.; Kumar Roy, P.; Děkanovský, L.; Sofer, Z.; Numan, A. 2D Heterostructures for Highly Efficient Photodetectors: From Advanced Synthesis to Characterizations, Mechanisms, and Device Applications. *Advanced Photonics Research* **2022**, *3* (8), 2100342. https://doi.org/10.1002/adpr.202100342.

(21) Gong, Y.; Lin, J.; Wang, X.; Shi, G.; Lei, S.; Lin, Z.; Zou, X.; Ye, G.; Vajtai, R.; Yakobson, B. I.; Terrones, H.; Terrones, M.; Tay, B. K.; Lou, J.; Pantelides, S. T.; Liu, Z.; Zhou, W.; Ajayan, P. M. Vertical and In-Plane Heterostructures from WS2/MoS2 Monolayers. *Nature Mater* **2014**, *13* (12), 1135–1142. https://doi.org/10.1038/nmat4091.

(22) Ye, L.; Li, H.; Chen, Z.; Xu, J. Near-Infrared Photodetector Based on MoS2/Black Phosphorus Heterojunction. *ACS Photonics* **2016**, *3* (4), 692–699. https://doi.org/10.1021/acsphotonics.6b00079.

(23) Viscardi, L.; Durante, O.; De Stefano, S.; Intonti, K.; Kumar, A.; Pelella, A.; Giubileo, F.; Kharsah, O.; Daniel, L.; Sleziona, S.; Schleberger, M.; Di Bartolomeo, A. Dominant N-Type Conduction and Fast Photoresponse in BP/MoS2 Heterostructures. *Surfaces and Interfaces* **2024**, 104445. https://doi.org/10.1016/j.surfin.2024.104445.

(24) Liu, W.; Yu, Y.; Peng, M.; Zheng, Z.; Jian, P.; Wang, Y.; Zou, Y.; Zhao, Y.; Wang, F.; Wu, F.; Chen, C.; Dai, J.; Wang, P.; Hu, W. Integrating 2D Layered Materials with 3D Bulk Materials as van Der Waals Heterostructures for Photodetections: Current Status and Perspectives. *InfoMat* **2023**, *5* (10), e12470. https://doi.org/10.1002/inf2.12470.

(25) Dong, Y.; Zhao, C.; Wang, H.; Jiang, Y.; Fang, Y.; Wang, J.; Duan, S.; Fu, X.; Miao, J.; Hu, W. Van Der Waals Integration of Two-Dimensional Materials and Bulk Semiconductors for Infrared Photodetection Technology. *MRS Bulletin* **2023**, *48* (9), 914–922. https://doi.org/10.1557/s43577-023-00599-0.

AIP Publishing Applied Physics Letters ACCEPTED MANUSCRIPT
This is the author's peer reviewed, accepted manuscript. However, the online version of record will be different from this version once it has been copyedited and typeset.
PLEASE CITE THIS ARTICLE AS DOI: 10.1063/5.0231243

(26) Di Bartolomeo, A. Graphene Schottky Diodes: An Experimental Review of the Rectifying Graphene/Semiconductor Heterojunction. *Physics Reports* **2016**, *606*, 1–58. https://doi.org/10.1016/j.physrep.2015.10.003.
(27) Jariwala, D.; Marks, T. J.; Hersam, M. C. Mixed-Dimensional van Der Waals Heterostructures. *Nature Mater* **2017**, *16* (2), 170–181. https://doi.org/10.1038/nmat4703.
(28) Tang, Q.; Zhong, F.; Li, Q.; Weng, J.; Li, J.; Lu, H.; Wu, H.; Liu, S.; Wang, J.; Deng, K.; Xiao, Y.; Wang, Z.; He, T. Infrared Photodetection from 2D/3D van Der Waals Heterostructures. *Nanomaterials* **2023**, *13* (7), 1169. https://doi.org/10.3390/nano13071169.
(29) Zhang, X.; Shao, J.; Su, Y.; Wang, L.; Wang, Y.; Wang, X.; Wu, D. *In-Situ* Prepared WSe2/Si 2D-3D Vertical Heterojunction for High Performance Self-Driven Photodetector. *Ceramics International* **2022**, *48* (20), 29722–29729. https://doi.org/10.1016/j.ceramint.2022.06.231.
(30) Wang, L.; Jie, J.; Shao, Z.; Zhang, Q.; Zhang, X.; Wang, Y.; Sun, Z.; Lee, S.-T. MoS2/Si Heterojunction with Vertically Standing Layered Structure for Ultrafast, High-Detectivity, Self-Driven Visible–Near Infrared Photodetectors. *Advanced Functional Materials* **2015**, *25* (19), 2910–2919. https://doi.org/10.1002/adfm.201500216.
(31) Mao, J.; Yu, Y.; Wang, L.; Zhang, X.; Wang, Y.; Shao, Z.; Jie, J. Ultrafast, Broadband Photodetector Based on MoSe2/Silicon Heterojunction with Vertically Standing Layered Structure Using Graphene as Transparent Electrode. *Adv Sci (Weinh)* **2016**, *3* (11), 1600018. https://doi.org/10.1002/advs.201600018.
(32) Lu, Z.; Xu, Y.; Yu, Y.; Xu, K.; Mao, J.; Xu, G.; Ma, Y.; Wu, D.; Jie, J. Ultrahigh Speed and Broadband Few-Layer MoTe2/Si 2D–3D Heterojunction-Based Photodiodes Fabricated by Pulsed Laser Deposition. *Advanced Functional Materials* **2020**, *30* (9), 1907951. https://doi.org/10.1002/adfm.201907951.
(33) Wu, D.; Guo, C.; Wang, Z.; Ren, X.; Tian, Y.; Shi, Z.; Lin, P.; Tian, Y.; Chen, Y.; Li, X. A Defect-Induced Broadband Photodetector Based on WS2/Pyramid Si 2D/3D Mixed-Dimensional Heterojunction with a Light Confinement Effect. *Nanoscale* **2021**, *13* (31), 13550–13557. https://doi.org/10.1039/D1NR03243G.
(34) Wu, E.; Wu, D.; Jia, C.; Wang, Y.; Yuan, H.; Zeng, L.; Xu, T.; Shi, Z.; Tian, Y.; Li, X. In Situ Fabrication of 2D WS_2/Si Type-II Heterojunction for Self-Powered Broadband Photodetector with Response up to Mid-Infrared. *ACS Photonics* **2019**, *6* (2), 565–572. https://doi.org/10.1021/acsphotonics.8b01675.
(35) Rahman, M.; Davey, K.; Qiao, S.-Z. Advent of 2D Rhenium Disulfide (ReS2): Fundamentals to Applications. *Advanced Functional Materials* **2017**, *27* (10), 1606129. https://doi.org/10.1002/adfm.201606129.
(36) Intonti, K.; Faella, E.; Kumar, A.; Viscardi, L.; Giubileo, F.; Martucciello, N.; Lam, H. T.; Anastasiou, K.; Craciun, M.; Russo, S.; Di Bartolomeo, A. Temperature-Dependent Conduction and Photoresponse in Few-Layer ReS_2. *ACS Appl. Mater. Interfaces* **2023**, *15* (43), 50302–50311. https://doi.org/10.1021/acsami.3c12973.
(37) Zhang, E.; Jin, Y.; Yuan, X.; Wang, W.; Zhang, C.; Tang, L.; Liu, S.; Zhou, P.; Hu, W.; Xiu, F. ReS_2-Based Field-Effect Transistors and Photodetectors. *Adv Funct Materials* **2015**, *25* (26), 4076–4082. https://doi.org/10.1002/adfm.201500969.
(38) Varghese, A.; Saha, D.; Thakar, K.; Jindal, V.; Ghosh, S.; Medhekar, N. V.; Ghosh, S.; Lodha, S. Near-Direct Bandgap WSe_2/ReS_2 Type-II Pn Heterojunction for Enhanced Ultrafast Photodetection and High-Performance Photovoltaics. *Nano Lett.* **2020**, *20* (3), 1707–1717. https://doi.org/10.1021/acs.nanolett.9b04879.
(39) Yim, C.; McEvoy, N.; Riazimehr, S.; Schneider, D. S.; Gity, F.; Monaghan, S.; Hurley, P. K.; Lemme, M. C.; Duesberg, G. S. Wide Spectral Photoresponse of Layered Platinum Diselenide-Based Photodiodes. *Nano Lett.* **2018**, *18* (3), 1794–1800. https://doi.org/10.1021/acs.nanolett.7b05000.
(40) Son, S. B.; Kim, Y.; Cho, B.; Choi, C.-J.; Hong, W.-K. Temperature-Dependent Electronic Charge Transport Characteristics at MoS2/p-Type Ge Heterojunctions. *Journal of Alloys and Compounds* **2018**, *757*, 221–227. https://doi.org/10.1016/j.jallcom.2018.05.034.
(41) Janardhanam, V.; Jyothi, I.; Yuk, S.-H.; Munkhsaikan, Z.; Choi, C.-J. Temperature-Dependent Interface Barrier Behavior in MoS2/n-GaN 2D/3D Heterojunction. *Materials Letters* **2021**, *296*, 129893. https://doi.org/10.1016/j.matlet.2021.129893.

AIP Publishing Applied Physics Letters ACCEPTED MANUSCRIPT
This is the author's peer reviewed, accepted manuscript. However, the online version of record will be different from this version once it has been copyedited and typeset.
PLEASE CITE THIS ARTICLE AS DOI: 10.1063/5.0231243

(42) Tung, R. T. Electron Transport at Metal-Semiconductor Interfaces: General Theory. *Phys. Rev. B* **1992**, *45* (23), 13509–13523. https://doi.org/10.1103/PhysRevB.45.13509.
(43) Moun, M.; Kumar, M.; Garg, M.; Pathak, R.; Singh, R. Understanding of MoS2/GaN Heterojunction Diode and Its Photodetection Properties. *Sci Rep* **2018**, *8* (1), 11799. https://doi.org/10.1038/s41598-018-30237-8.
(44) Janardhanam, V.; Jyothi, I.; Kim, Y.; Lee, S.-N.; Yun, H.-J.; Hong, W.-K.; Choi, C.-J. Carrier Conduction Mechanisms of WSe2/p-Type Ge Epilayer Heterojunction Depending on the Measurement Temperature and Applied Bias. *Journal of Alloys and Compounds* **2020**, *842*, 155843. https://doi.org/10.1016/j.jallcom.2020.155843.
(45) Roul, B.; Bhat, T. N.; Kumar, M.; Rajpalke, M. K.; Sinha, N.; Kalghatgi, A. T.; Krupanidhi, S. B. Barrier Height Inhomogeneities in InN/GaN Heterostructure Based Schottky Junctions. *Solid State Communications* **2011**, *151* (20), 1420–1423. https://doi.org/10.1016/j.ssc.2011.07.008.
(46) Mondal, S.; Halder, S.; Basak, D. Ultrafast and Ultrabroadband UV–Vis-NIR Photosensitivity under Reverse and Self-Bias Conditions by n^+-ZnO/n-Si Isotype Heterojunction with >1 kHz Bandwidth. *ACS Appl. Electron. Mater.* **2023**, *5* (2), 1212–1223. https://doi.org/10.1021/acsaelm.2c01668.
(47) Bao, C.; Chen, Z.; Fang, Y.; Wei, H.; Deng, Y.; Xiao, X.; Li, L.; Huang, J. Low-Noise and Large-Linear-Dynamic-Range Photodetectors Based on Hybrid-Perovskite Thin-Single-Crystals. *Advanced Materials* **2017**, *29* (39), 1703209. https://doi.org/10.1002/adma.201703209.
(48) Jo, B.; Seo, K.; Park, K.; Jeong, C.; Poornaprakash, B.; Lee, M.; Ramu, S.; Hahm, M. G.; Kim, Y. L. Trap-Assisted Monolayer ReSe2/Si Heterojunction with High Photoconductive Gain and Self-Driven Broadband Photodetector. *Front. Mater.* **2024**, *11*. https://doi.org/10.3389/fmats.2024.1354522.
(49) Zhou, C.; Zhang, S.; Lv, Z.; Ma, Z.; Yu, C.; Feng, Z.; Chan, M. Self-Driven WSe2 Photodetectors Enabled with Asymmetrical van Der Waals Contact Interfaces. *npj 2D Mater Appl* **2020**, *4* (1), 1–9. https://doi.org/10.1038/s41699-020-00179-9.
(50) Wang, Q.; Zhou, C.; Chai, Y. Breaking Symmetry in Device Design for Self-Driven 2D Material Based Photodetectors. *Nanoscale* **2020**, *12* (15), 8109–8118. https://doi.org/10.1039/D0NR01326A.
(51) Jia, C.; Wu, D.; Wu, E.; Guo, J.; Zhao, Z.; Shi, Z.; Xu, T.; Huang, X.; Tian, Y.; Li, X. A Self-Powered High-Performance Photodetector Based on a MoS2/GaAs Heterojunction with High Polarization Sensitivity. *J. Mater. Chem. C* **2019**, *7* (13), 3817–3821. https://doi.org/10.1039/C8TC06398B.
(52) Shin, G. H.; Park, J.; Lee, K. J.; Lee, G.-B.; Jeon, H. B.; Choi, Y.-K.; Yu, K.; Choi, S.-Y. Si–MoS2 Vertical Heterojunction for a Photodetector with High Responsivity and Low Noise Equivalent Power. *ACS Appl. Mater. Interfaces* **2019**, *11* (7), 7626–7634. https://doi.org/10.1021/acsami.8b21629.
(53) Smidstrup, S.; Markussen, T.; Vancraeyveld, P.; Wellendorff, J.; Schneider, J.; Gunst, T.; Verstichel, B.; Stradi, D.; Khomyakov, P. A.; Vej-Hansen, U. G.; Lee, M.-E.; Chill, S. T.; Rasmussen, F.; Penazzi, G.; Corsetti, F.; Ojanperä, A.; Jensen, K.; Palsgaard, M. L. N.; Martinez, U.; Blom, A.; Brandbyge, M.; Stokbro, K. QuantumATK: An Integrated Platform of Electronic and Atomic-Scale Modelling Tools. *J. Phys.: Condens. Matter* **2019**, *32* (1), 015901. https://doi.org/10.1088/1361-648X/ab4007.
(54) Jelver, L.; Stradi, D.; Stokbro, K.; Wedel Jacobsen, K. Schottky Barrier Lowering Due to Interface States in 2D Heterophase Devices. *Nanoscale Advances* **2021**, *3* (2), 567–574. https://doi.org/10.1039/D0NA00795A.
(55) Reshchikov, M. A.; Foussekis, M.; Baski, A. A. Surface Photovoltage in Undoped N-Type GaN. *Journal of Applied Physics* **2010**, *107* (11), 113535. https://doi.org/10.1063/1.3430979.
(56) Kilin, D. S.; Micha, D. A. Surface Photovoltage at Nanostructures on Si Surfaces: Ab Initio Results. *J. Phys. Chem. C* **2009**, *113* (9), 3530–3542. https://doi.org/10.1021/jp808908x.
(57) Munakata, C.; Matsubara, S. The Photovoltaic Observation of Semiconductor Surfaces. *J. Phys. D: Appl. Phys.* **1983**, *16* (6), 1093–1098. https://doi.org/10.1088/0022-3727/16/6/017.